



HAL
open science

High temperature behaviour of various natural building stones

Martin Vigroux, Javad Eslami, Anne-Lise Beaucour, Ann Bourgès, Albert Noumowé

► **To cite this version:**

Martin Vigroux, Javad Eslami, Anne-Lise Beaucour, Ann Bourgès, Albert Noumowé. High temperature behaviour of various natural building stones. *Construction and Building Materials*, 2021, 272, pp.121629. 10.1016/j.conbuildmat.2020.121629 . hal-04383418

HAL Id: hal-04383418

<https://hal.science/hal-04383418v1>

Submitted on 22 Jul 2024

HAL is a multi-disciplinary open access archive for the deposit and dissemination of scientific research documents, whether they are published or not. The documents may come from teaching and research institutions in France or abroad, or from public or private research centers.

L'archive ouverte pluridisciplinaire **HAL**, est destinée au dépôt et à la diffusion de documents scientifiques de niveau recherche, publiés ou non, émanant des établissements d'enseignement et de recherche français ou étrangers, des laboratoires publics ou privés.



Distributed under a Creative Commons Attribution - NonCommercial 4.0 International License

High Temperature Behaviour of Various Natural Building Stones

Martin Vigroux¹, Javad Eslami^{1,*}, Anne-Lise Beaucour¹, Ann Bourguès^{2,3}, Albert Noumowé¹

¹ *CY Cergy Paris Université, Laboratoire de Mécanique et Matériaux du Génie Civil, EA4114, F-95000 Cergy-Pontoise, France*

² *Laboratoire de Recherche des Monuments Historiques, Ministère de la Culture et de la Communication, 29 rue de Paris, 77420 Champs-sur-Marne, France*

³ *Sorbonne Universités, Centre de Recherche sur la conservation (CRC, USR 3224), Muséum national d'Histoire naturelle, Ministère de la Culture et de la Communication, CNRS, CP21, 36 rue Geoffroy-Saint-Hilaire, 75005 Paris, France*

* Corresponding author: javad.eslami@cyu.fr

HIGHLIGHTS.

Natural building stones used in historical monuments were tested facing high temperature exposure up to 1000 °C. TGA-DSC analyses allowed the identification of the main thermo-chemical reactions occurring under high temperature. Thermal linear expansion tests were conducted to assess the thermo-mechanical behaviour under high temperature. Mechanical properties have been evaluated after an exposure to heating-cooling cycles up to 800 °C.

ABSTRACT. The aim of this study is to investigate the effect of high temperature and identify important changes that occur when selected building stones (six french limestones and a sandstone) are laboratory-heated. Tests under high temperature such as thermogravimetric analysis, differential scanning calorimetry measurements but also thermal linear expansion tests were conducted in order to establish the thermo-chemical-mechanical behaviour of these materials when subjected to high temperature. Furthermore, these stones were exposed to four different heating-cooling cycles (200, 400, 600, 800 °C). Then, mechanical tests were performed to determine the evolution of compressive strength, tensile strength and dynamic elastic modulus.

KEY WORDS: high temperature, thermal expansion, mineralogy, thermal damage, mechanical properties, limestone, sandstone

39 1. Introduction

40 Fire has always been a major threat to building and consequences can then be dramatic. Since
41 natural stones have been used for a long time as building material in historical monuments, and are
42 still used as restoration material, a detailed understanding of thermal damage and failure mechanical
43 behaviour of these porous materials at elevated temperature is a key concern. Fire appears as one of
44 the main causes of built heritage weathering because it can generate irreversible damage with long-
45 lasting effects, in a very short period of time [1,2]. A well-known example for that is the recent fire
46 that devastated Paris' world-famous Notre-Dame Cathedral on April 15th 2019.

47 A fire exposure on natural building stones leads generally to irreversible changes in
48 microstructure [3–5] and consequently on physico-mechanical properties. These disorders may
49 compromise the structural integrity of the stone and increase the risk of instability of the entire
50 building. Then, many authors studied the effect of high temperature exposure on residual mechanical
51 properties on different types of stones [6–12]. Even if a general trend emerges indicating that
52 mechanical performances decrease along a rise in temperature, it is difficult to define clearly a
53 common evolution to all types of stones, and even for stones of the same type.

54 Natural stones are made up of one or different types of minerals. This suggests that stones are
55 very likely influenced by the high temperature behaviour of their constitutive minerals. Several studies
56 have been conducted to investigate the effect of mineralogical composition of the stones on their high
57 temperature sensitivity. Thus, calcite is the predominant mineral in limestones and the decarbonation
58 of calcium carbonate (CaCO_3) from 750 °C may constitute the main negative effect for carbonate
59 stones. Indeed, this thermo-chemical transformation involves a significant mass loss and the
60 subsequent hydration of calcium oxide (CaO) during cooling leads to an important volume change
61 resulting in stone alteration [9,11,13,14]. When exposed to fire, siliceous stones such as sandstones
62 can suffer thermal degradation that is mainly due to the α - β quartz transformation occurring at 573 °C.
63 This reversible change is associated with a sudden increase in volume that can generate microcracks at
64 grain boundaries [15–17].

65 Some authors have been interested in thermal expansion behaviour of different types of stones.
66 However, it is admitted that thermal damage of carbonate stones at temperatures up to 600 °C is
67 largely related to the strongly anisotropic thermal expansion of calcite that causes intergranular
68 microcracking [11,18,19]. Hence, it has been shown that crystals of calcite expand parallel and
69 contract perpendicular to crystallographic c-axis [20]. Moreover, siliceous stones are expected to
70 expand a little more than limestones due to the highest value of thermal expansion coefficient of
71 quartz [20,21]. Only a few works have been carried out trying to identify the main parameters
72 controlling the thermal expansion sensitivity of stones when exposed to high temperature [12,22,23]. It

73 appears that polymineralic stones are more sensitive because they are subjected to differential thermal
74 deformation due to thermal incompatibility of their components. Moreover, others parameters such as
75 initial porosity seems to play a main role: a high porosity may compensate the thermal expansion of
76 minerals to a certain degree [11]. In addition, grain size is defined as a main factor influencing on
77 thermal expansion [22] while its effect cannot be considered as important on different types of marbles
78 [11]. Consequently, there is a lack of knowledge on these elements and no consensus is established.
79 Moreover, the temperature ranges did not exceed 500 °C on most of the thermal expansion tests
80 conducted by other authors, and so do not reflect temperatures that can be encountered during real fire
81 situations.

82 Generally, the assessment of alteration level of stones induced by a fire exposure requires
83 destructive tests but the need for heritage preservation entails post-fire surveyors to rely upon non-
84 destructive tests, among which P-wave velocity. Indeed, the evolution of this latter parameter can give
85 interesting information about how the material is affected by elevated temperatures. Based on
86 literature review, lots of authors consider this parameter as a good indicator to evaluate the
87 temperature-induced damage of the stone [9,24–29].

88 Thereby, the purpose of this heat-laboratory-based work is to investigate the effect of high
89 temperature exposure on different types of porous stones, and determine the governing parameters on
90 fire stability. Therefore, seven stones with different mineralogy and various physical characteristics
91 are tested. First of all, ThermoGravimetric analysis (TGA) and Differential Scanning Calorimetric
92 (DSC) measurements were carried out in order to investigate the main related mineral reactions and
93 their consequences on stones stability. Moreover, thermal linear expansion tests were performed to
94 establish the thermo-mechanical behaviour of these materials when subjected up to 1000 °C. Thermal
95 damage was evaluated after exposure to heating-cooling cycles at different temperature levels by the
96 assessment of residual deformation. Heating-cooling cycles refer to a three-stage program consisting
97 in (1) rising up to the target temperature at a constant rate (4 °C.min⁻¹), then (2) a one-hour isotherm
98 stage at the target temperature and finally (3) a cooling phase to reach back to the room temperature.
99 Then, damage evolution is quantified through change measurements of physico-mechanical properties
100 (compressive strength, tensile strength, P-wave velocity, and dynamic elastic modulus) on heated
101 specimens after different heating-cooling cycles (200, 400, 600, 800 °C). Finally, this study highlights
102 the intrinsic parameters governing the high temperature sensitivity of these stones when exposed to
103 high temperature up to 1000 °C.

104 **2. Materials and methods**

105 **2.1 Materials**

106 The seven stones used in this study correspond to fresh samples coming from active quarries,
107 located in different regions of France. Six of them are classified as limestones: Massangis (MA), Lens
108 (LS), Euville (EUV), Migné (MI), Saint Maximin (MX), Savonnières (SA) while the seventh one is a
109 sandstone from North-East of France: Grès des Vosges (GR). These stones have been chosen because
110 they have been widely used in the construction of historical monuments and are still used for
111 restoration purposes [30–34]. Moreover, they present a large variety of physical, mechanical and
112 petrographic properties, allowing to understand the influence of these intrinsic parameters on the high
113 temperature sensitivity.

114 **2.2 Experimental procedures**

115 2.2.1 Characterization tests

116 X-ray diffraction (XRD) analyses carried out on powder samples allow to identify the
117 mineralogical composition of these materials. In addition, a microscopic study was conducted with a
118 polarized light microscope Leica DM2700M. Image analysis performed on thin-section micrographs
119 allows the determination of the average grain size for each stone. Moreover, the relative composition
120 of the different constitutive phases of the stones is obtained thanks to a 300 point-counting analysis
121 performed on thin sections with PetrogLite. Therefore, the identification of these selected stones
122 according to Dunham's classification [35] for carbonate rocks, and to Dott classification system [36]
123 for siliceous detrital rocks is possible.

124 With the aim of investigating the effect of different levels of high temperature on the studied
125 stones, laboratory tests were performed at initial state, and then after these four heating-cooling cycles
126 (within two hours after the heated specimens reached back the room temperature) to analyze the
127 evolution of physico-mechanical properties as a function of temperature.

128 Therefore, uniaxial compression test was carried out on three cylindrical $\Phi 40 \times 80$ mm
129 specimens according to standards NF EN 1926 [37] in order to determinate the compressive strength
130 (R_C). A constant rate ($100 \mu\text{m}\cdot\text{min}^{-1}$) was applied with an electromechanical static load cell Intron
131 Press 30 kN. Moreover, some specimens were equipped with four strain gauges in order to measure
132 the axial and longitudinal strain only at initial state. The loading path corresponds to a uniaxial-cyclic
133 compression with increasing unloading-reloading cycles. Hence, the tangential initial Young's
134 modulus and Poisson's ratio (ν) were calculated from the linear portions of strain-stress curves. Then,
135 Brazilian indirect tensile test was achieved with the same Instron device on four cylindrical $\Phi 40 \times 40$
136 mm specimens according to standards NF P 94-422 [38] to obtain the tensile strength (R_T). The strain

137 rate was maintained constant (1 kN.min⁻¹) until the failure. These two mechanical tests were carried
138 out for each stone at initial state and after the four different heating-cooling cycles.

139 The water porosity under vacuum technique was used to determine the open porosity (N_T) and
140 the real density (ρ). This test was performed according to standard NF EN 1936 [39].

141 Measurements of P-wave velocity (V_P) were performed using a Pundit7, a wave propagation
142 test device from Pundit Lab, according to standards NF EN 14-579 [40]. The frequency of the solitary
143 pulse in this experiment was 54 kHz and two adequate piezoelectric detectors were used. Petroleum
144 jelly was applied as coupling product between transducers and sample surface to ensure a satisfying
145 wave propagation. The average values for each stone are based on 60 samples ($\Phi 40 \times 80$ mm) for
146 initial state and based on 10 samples after each high temperature treatment (40 specimens in total per
147 stone). This test gives information on microcracking state inside the sample and the dynamic elastic
148 modulus (E_{dyn}) is thus determined from equation 1:

$$E_{dyn} = \rho \cdot V_P^2 \cdot \frac{(1 + \nu)(1 - 2\nu)}{(1 - \nu)} \quad (1)$$

149 2.2.2 Tests under high temperature

150 In order to investigate the mass and heat flux evolution during heating, thermogravimetric
151 (TGA) and differential scanning calorimetry (DSC) analyses were conducted using a STA 449 F1
152 Jupiter device developed by Netzsch. Three tests are carried out for each type of stone. Stone
153 fragments, previously dried in an oven at 80 °C for 72 hours, are ground into powder. Then, a small
154 amount of material (80 mg) is introduced into an alumina crucible. The heating program consists of a
155 temperature increase from room temperature up to 1000 °C at a rate of 10 °C.min⁻¹, under an inert
156 atmosphere (nitrogen).

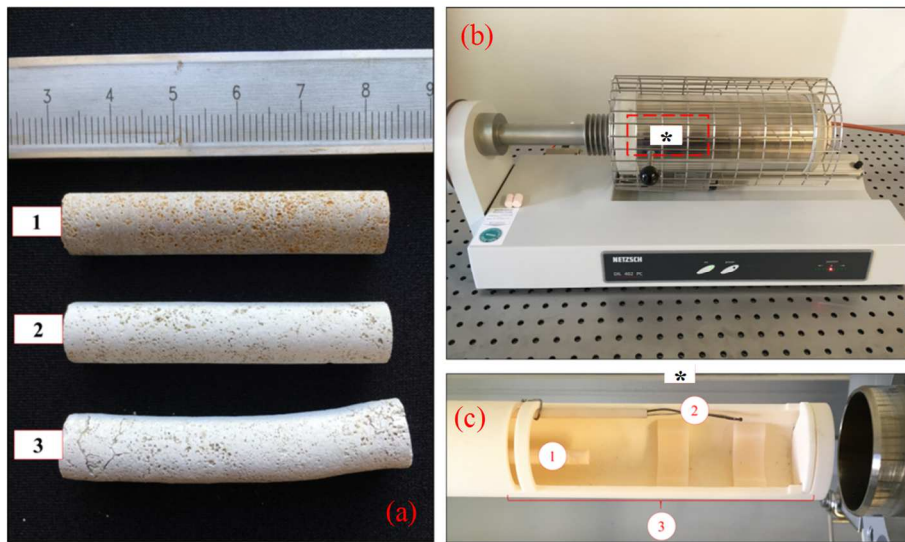
157 Moreover, the thermal linear deformation was recorded using a Pushrod dilatometer DIL 402 C
158 by Netzsch (Figure 1). These tests are performed on three cylindrical samples ($\Phi 10 \times 50$ mm in
159 length), previously dried in an oven at 80 °C for 72 hours. Then, the sample is introduced into the
160 specimen holder inside the furnace. A 25 cN force is applied to the sample by a pushrod to hold it
161 against the support. A connected displacement transducer (LVDT) allows the measurement of thermal
162 expansion during heating-cooling cycles. A thermocouple is also positioned on the surface of the
163 sample for temperature monitoring (Figure 1 - c). With the aim of considering the expansion
164 contribution of the sample holder and pushrod, a prior calibration test is carried out using a control
165 sample (alumina) provided by Netzsch. Three samples for each type of stone are subjected to four
166 different heating-cooling cycles, where the maximum temperature reaches 250, 500, 750 and 1050 °C.

167 The heating rate is set at 4 °C.min⁻¹, which allows the temperature homogenisation within the
168 specimen, and thus not to generate a significant thermal gradient. The thermal linear deformation is
169 recorded during the heating and cooling phases in order to evaluate the effect of different levels of
170 high temperature on the induced deformation.

171 The thermal linear expansion coefficient (α), depending on temperature, is then calculated using
172 the following equation 2:

$$\alpha = \frac{1}{\Delta T} \times \frac{\Delta L}{L_0} \quad (2)$$

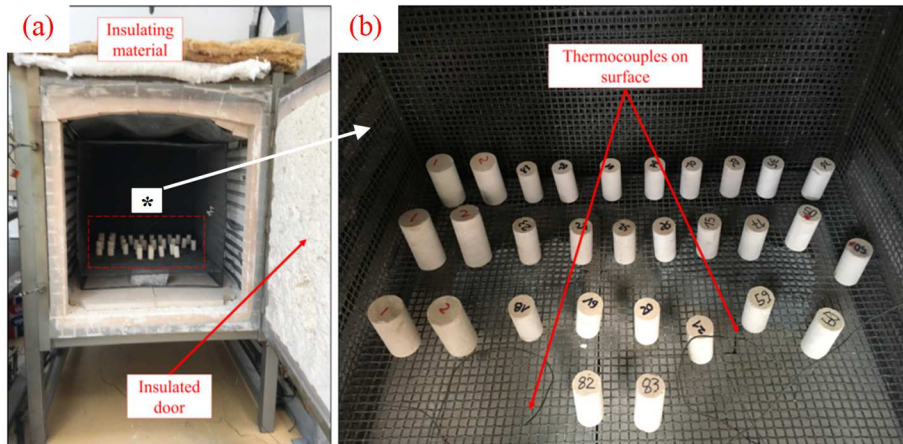
173 Where α : thermal linear expansion coefficient in °C⁻¹; ΔT : thermal gradient in °C; ΔL : length
174 change in m; L_0 : initial length of the specimen in m



175
176 *Figure 1 - (a) Samples used for the thermal linear expansion test: (1) before the test, (2) at the end of*
177 *the test, (3) 24 hours after the end of the test; (b) NETZSCH DIL 402 C dilatometer; (c) Device*
178 *features: (1) displacement sensor, (2) thermocouple, (3) sample holder*

179 2.2.3 Heating-cooling cycles

180 An electric furnace with a 1.35 m³ capacity was used (1.12 m long, 1.20 m in depth and 1.00 m
181 high). The two side walls are equipped with heating resistors and a ventilator is located at the back of
182 the furnace to maintain a homogeneous temperature distribution. Type-K thermocouples were
183 positioned at different positions to verify these conditions (Figure 2).



184

185

Figure 2 - (a) Furnace configuration and (b) samples location inside

186

187

188

189

190

191

192

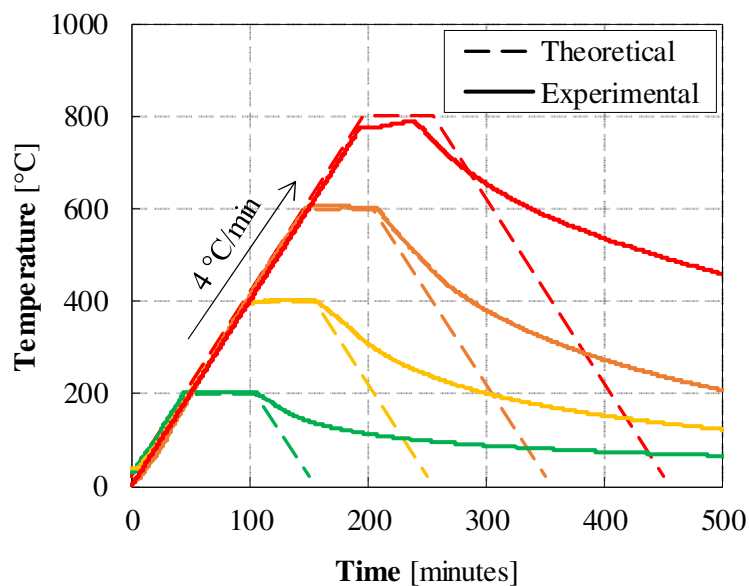
193

194

195

196

Four different high temperature treatments were applied on samples through heating-cooling cycles: from room temperature up to 200, 400, 600 and 800 °C. Each thermal treatment includes a 4 °C.min⁻¹ heating phase up to target temperature, then a one-hour isotherm stage and finally a semi-forced cooling phase (Figure 3). The parameters of these heating-cooling cycles are based on the RILEM recommendations [41], which consider the size of the heated samples (cylindrical $\Phi 40 \times 80$ mm specimens). Although this standard refers only to concrete samples, we assume it could be applied considering natural stones are porous material, but also because there is not existing standard about laboratory-heating parameters for stones. Since the main objective is to establish the trends of evolution of the material properties as a function of temperature, it is essential to ensure the temperature homogeneity throughout the sample and therefore to limit cracks development due to thermal gradients.



197

198

Figure 3 - Thermal profiles of the different heating-cooling cycles

199

2.2.4 Tests after high temperature exposure

200

201

202

A summary of the experimental high-temperature characterization program is presented in Table 1. It summarizes for each stone, the number and dimension of samples used per type of test, associated with the four thermal cycles.

203

Table 1 - Overview of the experimental work

	Type of test	Parameters	Samples	Number of samples tested			
				200 °C	400 °C	600 °C	800 °C
HT	TGA/DSC	mass, Φ_{thermal}	80 mg (powder)	3 (up to 1000 °C)			
	Linear thermal expansion	$\Delta L/L_0$, α	$\Phi 10 \times 50$ mm	3 for each cycle			
After HT	Compressive strength	R_C	$\Phi 40 \times 80$ mm	3	3	3	3
	Tensile strength	R_T	$\Phi 40 \times 40$ mm	4	4	4	4
	P-wave velocity	V_P , E_{dyn}	$\Phi 40 \times 80$ mm	10	10	10	10

204

3. Results and discussion

205

3.1 Stones description at initial state

206

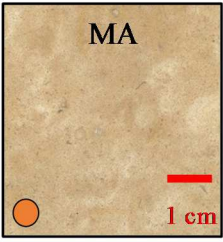
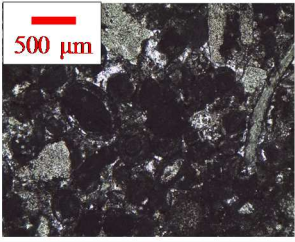
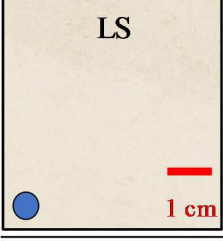
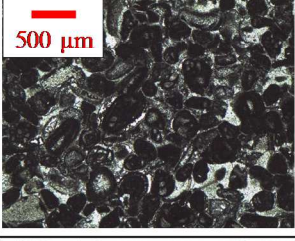
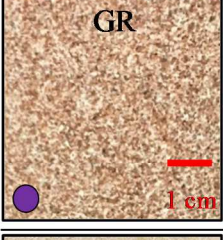
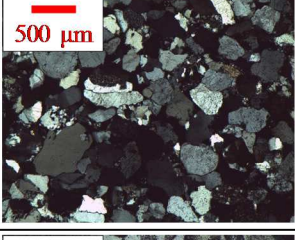
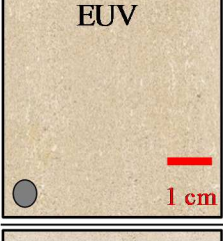
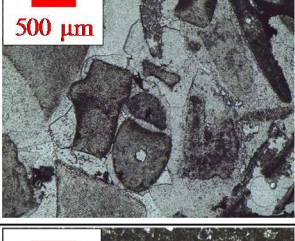
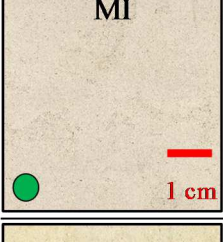
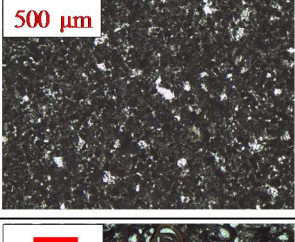
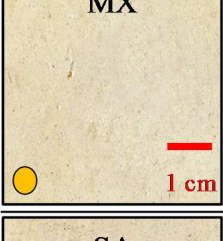
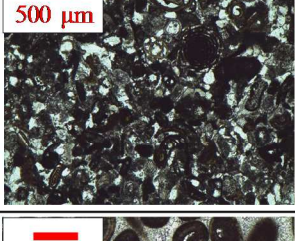
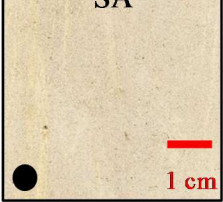
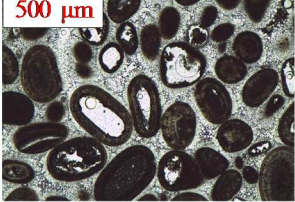
207

208

209

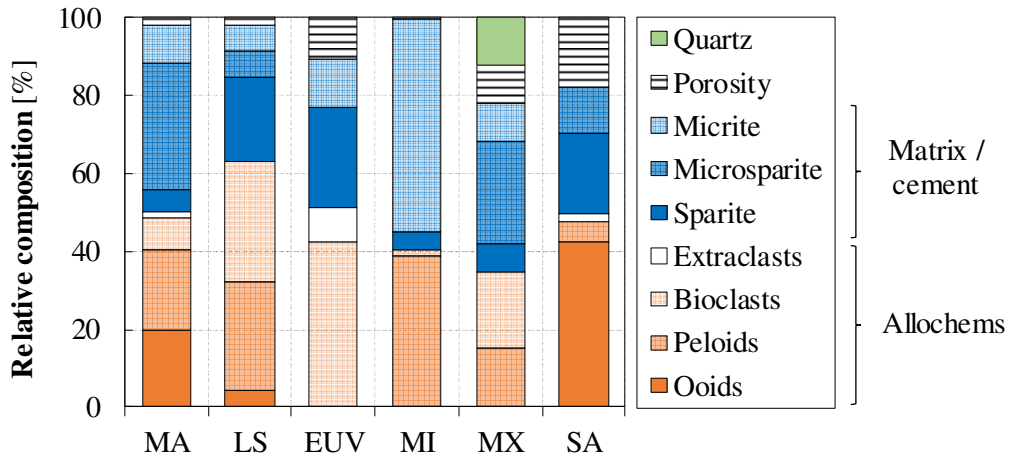
210

MA limestone consists of a dominant calcite-dolomite phase and a small amount of quartz. LS, EUV, MI and SA limestones are monophasic and composed only of calcite, while MX stone is also mainly made up of calcite but contains some quartz grains (~ 15 %). The sandstone GR has a high quartz-content, with traces of iron oxide, and a very low clay-content matrix. Figure 4 summarizes the main petrographic characteristics of these seven stones.

Macroscopic (a)	Microscopic (b)	Mineralogy (c)	Grain size [μm] (d)	Classification (e)
 <p>MA</p>		<p>Calcite, dolomite, quartz</p>	<p>($\pm \sigma$: <i>std</i>)</p> <p>625 ± 392 μm</p>	<p>Oolitic/peloidal grainstone</p>
 <p>LS</p>		<p>Calcite</p>	<p>300 ± 89 μm</p>	<p>Bioclastic grainstone</p>
 <p>GR</p>		<p>Quartz, iron oxide, clay</p>	<p>391 ± 94 μm</p>	<p>Feldspathic litharenite</p>
 <p>EUV</p>		<p>Calcite</p>	<p>1337 ± 610 μm</p>	<p>Crinoidal grainstone</p>
 <p>MI</p>		<p>Calcite</p>	<p>68 ± 17 μm</p>	<p>Peloidal packstone</p>
 <p>MX</p>		<p>Calcite, quartz</p>	<p>309 ± 131 μm</p>	<p>Bioclastic packstone</p>
 <p>SA</p>		<p>Calcite</p>	<p>526 ± 180 μm</p>	<p>Oolitic grainstone</p>

212 *Figure 4 - Description of the different stones at initial state: (a) macroscopic images, (b) micrographs*
213 *from thin-section observations on transmitted light microscope, (c) main minerals identified by XRD*
214 *analysis (predominant minerals in bold), (d) average grain size and standard deviation obtained from*
215 *image analysis, (e) Dunham's classification for carbonate rocks, and Dott's classification for siliceous*
216 *detrital rocks*

217 MA limestone is defined as an oolitic/peloidal grainstone, predominantly composed of peloids
218 and ooids in a microsparite matrix that makes a significant part of the sample. Some bioclasts are also
219 observable (echinoderms, bivalves). LS stone is classified as a bioclastic grainstone containing in
220 equal proportions bioclasts (foraminifera, echinoderms) and peloids supported in a sparite/micrite
221 matrix. However, sparite crystals are more present and rarely exceed 200 μm . GR sandstone is a
222 felspathic litharenite mainly made up of quartz grains ($\sim 400 \mu\text{m}$). The matrix proportion in the sample
223 is very low and consists of a mix of clay minerals (illite and kaolinite). EUV limestone is a bioclastic
224 and more precisely crinoidal grainstone with a coarse-grained texture. Multi-millimetric fragments
225 (500 to 2800 μm) of crinoid stem form a main part of the sample with a syntaxial overgrowth calcite
226 crystals matrix. In contrast, MI stone is a peloidal packstone composed almost exclusively of small
227 peloids (50 to 100 μm) in a very fine micrite matrix. MX limestone corresponds to a bioclastic
228 packstone where the binder phase is made up of a mix of sparite crystals, microsparite and micrite.
229 Nevertheless, sparitic cement is less observable and calcite crystals do not exceed 200 μm . Allochems
230 are divided in three groups: bioclasts through foraminifera species (miliolidae), micritized peloids but
231 also quartz minerals. SA limestone is an oolitic grainstone containing a large proportion of ooids (300
232 to 600 μm) associated with a sparite/microsparite matrix. These differences in terms of petrographic
233 features are also reflected with the average grain size. On the one hand, EUV limestone displays a very
234 large and heterogeneous grain size distribution ($1337 \pm 610 \mu\text{m}$). On the other hand, MI limestone
235 presents an average grain size centered in very low values, less than 100 μm ($68 \pm 17 \mu\text{m}$). The other
236 stones can be divided in two sub-groups: the first one showcasing an average grain size close to 300
237 μm (LS, GR, MX) while the second one (MA, SA) describes a less homogeneous distribution with
238 higher values $\sim 600 \mu\text{m}$. Figure 5 shows specifically the relative composition of the different
239 constitutive phases of the six limestones.



240

241

Figure 5 - Relative composition of the different constitutive phases of limestones

242

These seven stones differ from each other by their mineralogical composition, texture and thus also with different physical and mechanical properties. Table 2 lists the main characteristics of these stones at initial state. Then, SA, MX and MI limestones have similar properties: high porosity greater than 25 %, accompanied by lower mechanical strength (R_C ranging from 10 to 20 MPa). GR, EUV and LS are less porous (~ 15 %), but present disparities in mechanical properties, with R_C ranging from 20 to 47 MPa. MA limestone, with the lowest porosity (11.2 ± 0.5 %), is the stone having the highest density and mechanical properties (74.5 ± 1.5 MPa for R_C and 8.7 ± 0.7 MPa for R_T).

248

249

Table 2 - Main physical and mechanical properties of stones at initial state - N_T (%): open porosity; ρ (kg.m^{-3}): real density; R_C (MPa): compressive strength; R_T (MPa): tensile strength; V_P (m.s^{-1}): P-wave velocity; ν (-): Poisson's ratio; E_{dyn} (GPa): dynamic elastic modulus

250

251

Parameters	MA	LS	GR	EUV	MI	MX	SA
N_T [%]	11.2 \pm 0.5	15.4 \pm 0.8	15.7 \pm 2.2	17.2 \pm 0.4	26.8 \pm 0.8	29.7 \pm 1.2	30.7 \pm 1.3
ρ [kg.m^{-3}]	2391 \pm 12	2252 \pm 23	2220 \pm 58	2209 \pm 15	1949 \pm 22	1791 \pm 23	1786 \pm 25
R_C [MPa]	74.5 \pm 1.5	27.5 \pm 1.5	46.8 \pm 1.6	20.0 \pm 0.5	20.1 \pm 3.1	15.5 \pm 1.2	9.4 \pm 0.6
R_T [MPa]	8.7 \pm 0.7	5.3 \pm 0.4	5.2 \pm 0.6	3.5 \pm 0.2	2.7 \pm 0.4	2.0 \pm 0.1	1.6 \pm 0.1
V_P [m.s^{-1}]	4941 \pm 192	4380 \pm 172	3067 \pm 195	3665 \pm 359	3138 \pm 95	2971 \pm 124	2984 \pm 119
ν [-]	0.28 \pm 0.03	0.28 \pm 0.03	0.37 \pm 0.04	0.26 \pm 0.03	0.24 \pm 0.02	0.28 \pm 0.03	0.29 \pm 0.03
E_{dyn} [GPa]	45.0 \pm 1.4	31.8 \pm 1.9	16.9 \pm 2.5	23.3 \pm 1.1	15.4 \pm 1.1	11.8 \pm 0.8	11.8 \pm 0.9

252

3.2 Tests under high temperature

3.2.1 Thermogravimetric (TGA) and Differential Scanning Calorimetry (DSC) analyses

Figure 6 shows the evolution of relative mass and heat flux for the seven studied stones as a function of temperature up to 1000 °C. The general trend for this six limestones is a stable thermal phase until 750 °C where the decarbonation of calcite ($\text{CaCO}_3 \rightarrow \text{CaO} + \text{CO}_2$) occurs and leads to an approximately 44 % mass loss when the chemical reaction is complete (930 °C) [9,42]. This mass loss is associated with a large endothermic peak at 900 °C due to the release of CO_2 . However, it should be noted that MX limestone has a mass loss slightly lower than 44 %, which can be explained by its small quartz-content, resulting in a lower calcite-content in comparison with the other limestones.

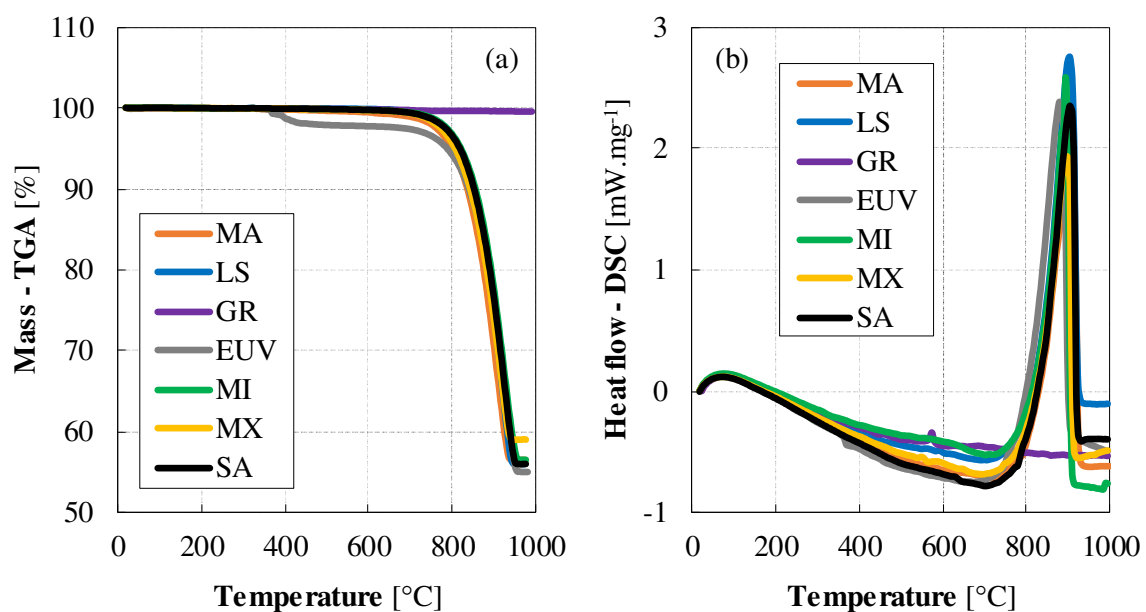
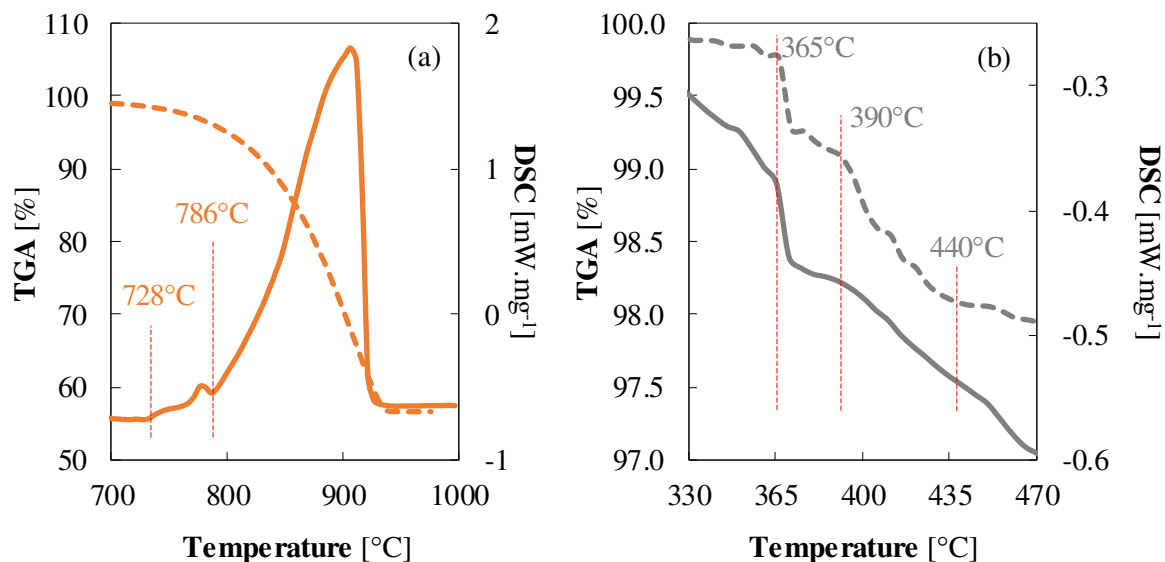


Figure 6 - (a) TGA and (b) DSC curves

In addition, EUV limestone presents an early mass loss (~ 2 %) which appears at 365 °C and stabilizes at 440 °C (Figure 7 - b). [43] observed a similar phenomenon on the same limestone, and suggested the hypothesis of the combustion of a small quantity of organic matter. Moreover, in his thesis work, [44] also obtained a slight mass loss for a limestone at this temperature interval. The analysis of the emitted gas at these precise temperatures shows a spectral signature corresponding to CO_2 . Consequently, he also attributed this mass loss to the initial presence of organic matter and its combustion. [45] gave the same explanation of organic compound combustion for specific carbonate rocks that they investigated.

Furthermore, the presence of dolomite in MA limestone is observable through its two-stage decomposition reaction ($\text{CaMg}(\text{CO}_3)_2 \rightarrow \text{CaCO}_3 + \text{MgO} + \text{CO}_2 \rightarrow \text{CaO} + \text{MgO} + 2 \text{CO}_2$) [9,46] which is firstly reflected in a slight peak in DSC, starting at 728 °C and ending at 786 °C (Figure 7 - a).

275 Concerning GR sandstone, it does not show any significant mass loss since the α - β phase
 276 transition of quartz at 573 °C is not associated with a loss of matter [13,17,47,48]. However, an
 277 endothermic peak is observable at 573 °C in DSC, and is attributed to this polymorphic transformation
 278 of quartz.

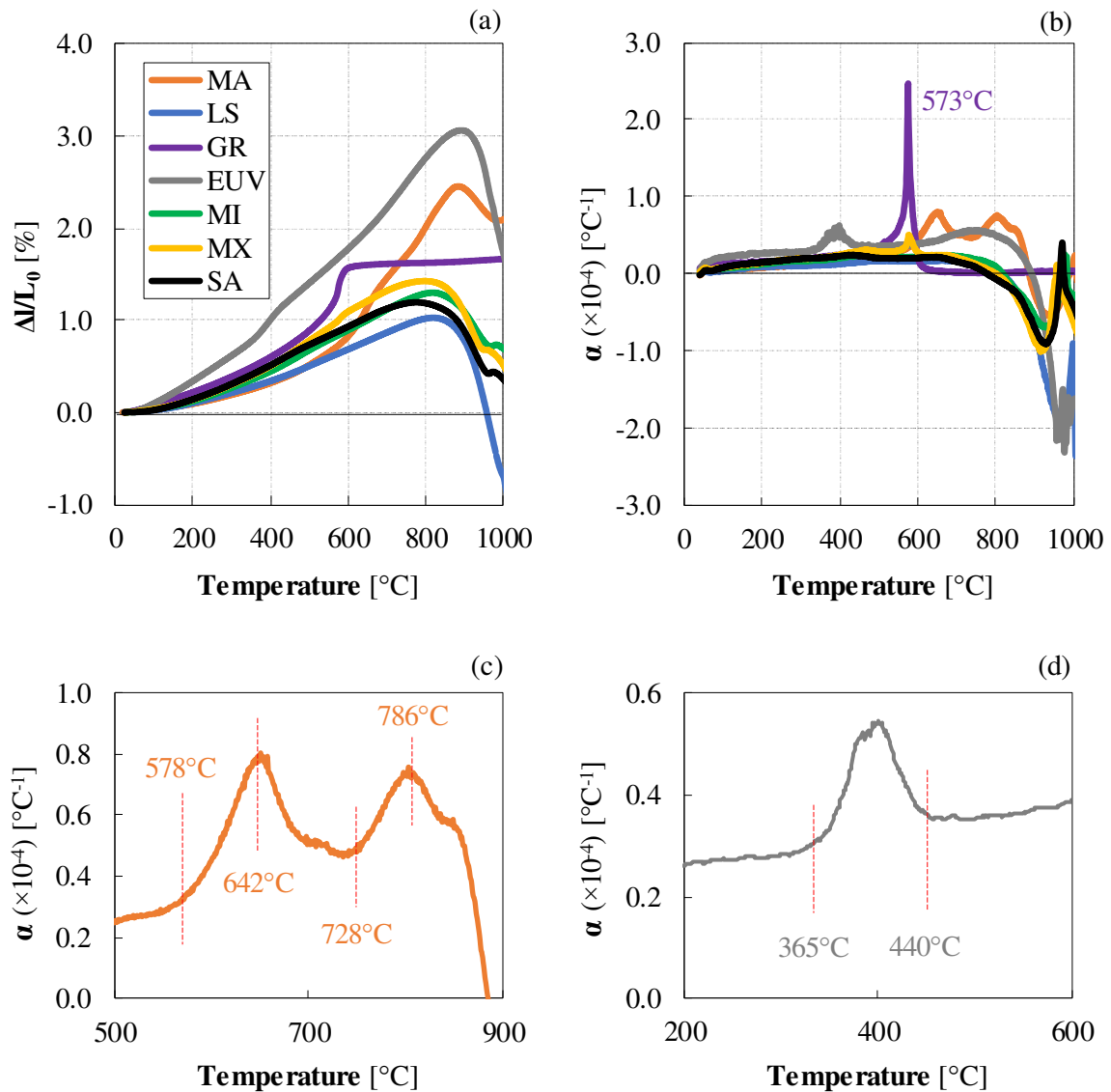


279
 280 *Figure 7 - Detailed TGA-DSC curves for (a) MA and (b) EUV limestones (dotted lines for TGA, solid*
 281 *lines for DSC)*

282 3.2.2 Thermal linear deformation

283 The thermal linear deformation during the heating phase up to 1000 °C is shown in Figure 8 - a
 284 for the different stones. The deformation induced by a rise in temperature corresponds essentially to an
 285 expansion of the specimen. This evolution is not linear with temperature and is governed by the
 286 thermal behaviour of the constitutive minerals of the stone. In addition, petrophysical factors such as
 287 initial porosity, grain size and texture can play a major role in the amplitude of deformation
 288 [11,12,49].

289 Thus, EUV limestone expands the most among all the stones. It is characterized by an
 290 expansion of 1.0 % at 400 °C and then reaches its maximum value (3.0 %) at 900 °C. The other
 291 limestones present a thermal expansion less important than EUV: ~ 0.5 % at 400 °C, and between 0.8
 292 and 1.1 % at 600 °C. Nevertheless, and despite different amplitudes, the general trend for limestones is
 293 similar and consists in a gradual expansion to reach a maximum value around 880 °C where a
 294 contraction phase starts, caused by the release of CO₂ during the dissociation of calcite.



295
 296 *Figure 8 - (a) Thermal linear deformation, (b) Thermal linear expansion coefficient of the different*
 297 *stones and detailed curves of (c) MA and (d) EUV limestones*

298 The expansion values displayed by EUV stone, which are significantly higher than other stones,
 299 can be explained by its wide multi-millimetric grain size distribution. It can be assumed that with
 300 larger grains, there is less surface area or joints between the grains which apply a buffering effect and
 301 absorb thermal deformation. MI, MX and SA limestones, with the higher porosity (~ 25-30 %), have
 302 the lowest deformation values. However, their different texture (grain size and grain arrangement),
 303 where MI has a fine micrite matrix and small grains, in opposition to SA stone, composed of bigger
 304 ooids, seem to play only a secondary role in thermal deformation in this case. The initial porosity of
 305 these stones ($26.8 \pm 0.8 \%$ for MI; $30.7 \pm 1.3 \%$ for SA) then appears to be a determining factor, void
 306 spaces allowing accommodations of the internal volume expansion. The thermal linear deformation of
 307 GR sandstone displays a different evolution. It is divided into two parts: a first phase where the

308 expansion gradually evolves up to 573 °C, and then a second phase where the deformation remains
309 stable (1.6 %) up to 1000 °C.

310 The evolution of thermal linear expansion coefficient is shown in Figure 8 - b. This evolution
311 can be directly linked with the presence of some specific minerals. Indeed, thermo-chemical
312 transformations of minerals, associated or not with a mass loss, can disturb the evolution of the
313 thermal deformation, and so cause a sudden expansion or contraction of the sample.

314 The evolution of this coefficient for LS, MI, MX and SA limestones is very similar. First of all,
315 a first phase is observable where this coefficient increases slightly and gradually to reach a quasi-
316 stable value between 400 and 700 °C ($\alpha_{LS} = 17 \times 10^{-6} \text{ °C}^{-1}$, $\alpha_{MI} = 22 \times 10^{-6} \text{ °C}^{-1}$, $\alpha_{MX} = 26 \times 10^{-6} \text{ °C}^{-1}$, α_{SA}
317 $= 19 \times 10^{-6} \text{ °C}^{-1}$). A second phase starts around 700 °C, due to the beginning of calcite decarbonation,
318 and presents a decrease of α , to reach negative values at 800 °C: this reflects an inversion of the
319 deformation kinetics where a contraction phase takes place instead of an expansion phase. This
320 decrease towards negative values continues until the end of the calcite decomposition (930 °C).

321 A very slight change in the slope of the thermal deformation for EUV limestone occurring at ~
322 400 °C, appears much more clearly by displaying thermal expansion coefficient (Figure 8 - d). Indeed,
323 after a rather stable evolution of this coefficient up to 350 °C ($\alpha = 25 \times 10^{-6} \pm 4 \times 10^{-6} \text{ °C}^{-1}$), a peak is
324 identifiable between 365 and 440 °C, with a maximum ($\alpha = 60 \times 10^{-6} \text{ °C}^{-1}$) located at 400 °C. This
325 temperature range corresponds perfectly to the one already mentioned in the mass evolution (TGA).
326 The combustion of a small proportion of organic matter could explain this mass loss, and resulting
327 mechanically in a sudden change in the kinetics of deformation. Although a mass loss is generally
328 accompanied by a contraction (as it has been shown in the decarbonation of calcite), it can be assumed
329 that this mass loss causes a microcracking development leading to an expansion: bioclasts containing
330 organic matter are shrinking while the majority of sparite crystals are expanding, which creates
331 deformation incompatibilities that microcrack the matrix.

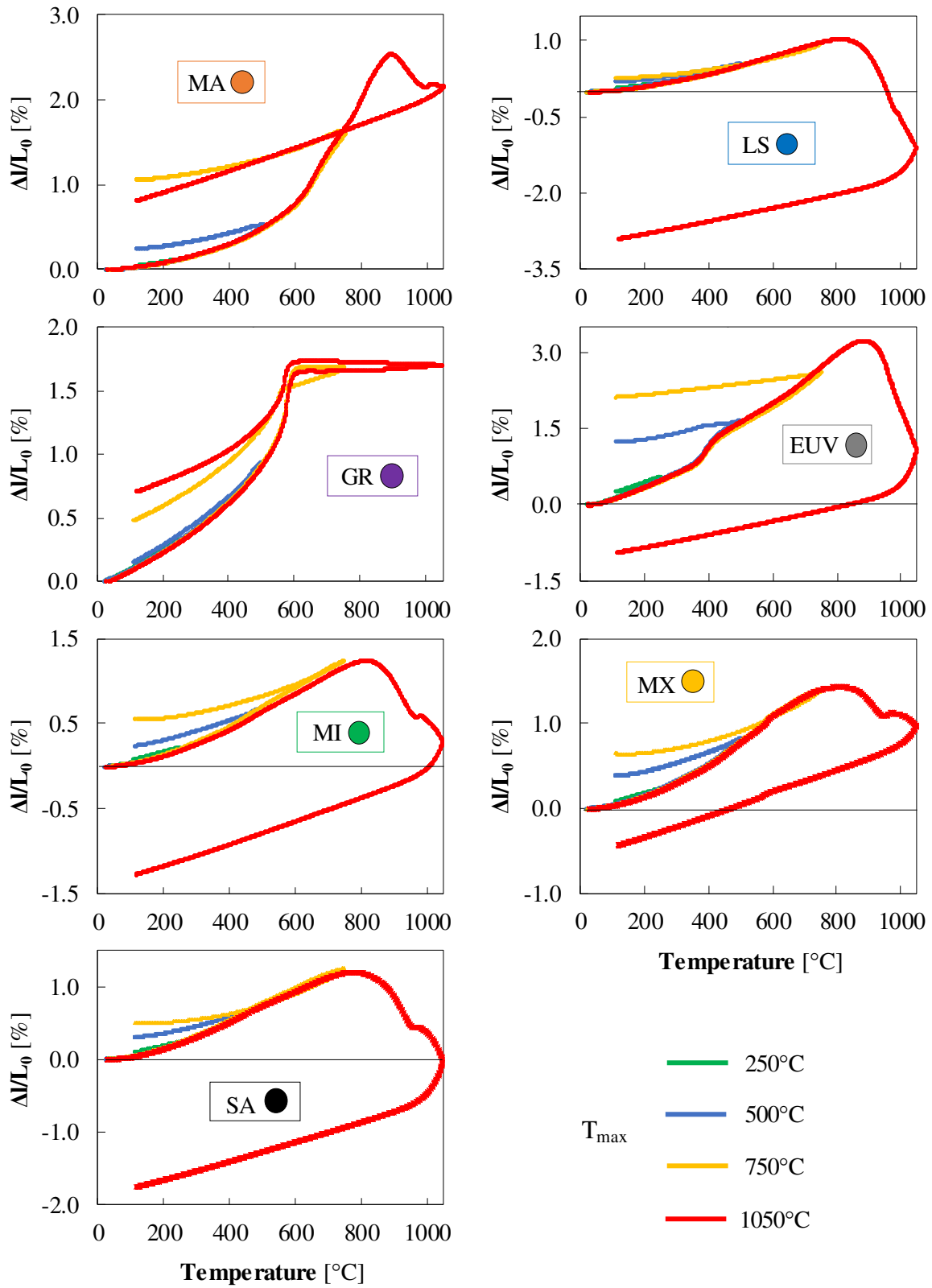
332 The presence of quartz minerals in GR sandstone and MX limestones results in a sudden peak at
333 573 °C. This peak even reaches a maximum value of $250 \times 10^{-6} \text{ °C}^{-1}$ for GR sandstone, while it does
334 not exceed $50 \times 10^{-6} \text{ °C}^{-1}$ for MX. The polymorphic transformation of quartz α - β is reversible and is
335 accompanied by a sudden increase in volume, about 5.7 % according to [20].

336 Two peaks can be observed for MA limestone (Figure 8 - c), where the maximum values are
337 located at 642 °C and 786 °C. As previously discussed, MA limestone contains mainly calcite and
338 dolomite, but also traces of quartz. Thus, the first peak, initiated at 578 °C, is assumed to be the
339 consequence of microcracking generated by the polyphasic mineralogical composition of this stone.
340 Indeed, differential thermal expansion seem to occur with minerals presenting different thermal
341 behaviours. Moreover, its low porosity ($N_T \sim 11 \%$) does not allow it to absorb the induced expansion.

342 The temperatures associated with the second peak (initiation at 728 °C and maximum at 786 °C)
343 match perfectly with those identified in the DSC curves, highlighting the early decomposition of
344 dolomite. However, the decomposition of carbonates usually induces shrinkage and therefore a
345 decrease in the coefficient α . Thus, this peak could be the result of dolomite decomposition, but also
346 mostly due to the damage induced through microcracks development, caused by the incompatibility of
347 deformation between the shrinkage of dolomite grains, and the expansion of calcite grains.

348 High temperature exposure usually leads to a permanent deformation. This thermal deformation
349 after a high temperature exposure characterizes the intensity of the thermal damage generated and
350 highlights the thermal sensitivity of the stone. The evaluation of residual strain can be used as a
351 quantitative expression of thermally induced damage [11]. Figure 9 aims to highlight the damage
352 induced by different levels of high temperature, and thus determine the critical maximum temperature
353 beyond which the stone is irreparably altered. Thus, the selected stones are subjected to four thermal
354 treatments (250, 500, 750 and 1050 °C) where the deformation is recorded during both heating and
355 cooling phases. The residual thermal deformation of the sample is then experimentally defined as the
356 difference in deformation between the initial state and after cooling. These results are individually
357 presented for each stone in Figure 9 while Figure 10 compares the thermal residual deformation of all
358 the stones at different temperature levels.

359 LS, EUV, MI, MX and SA limestones present a same characteristic: their residual deformation
360 induced by a 250, 500 and 750 °C cycles remain positive (expansion) while a heating-cooling cycle at
361 1050 °C leads to a negative residual deformation (contraction). In contrast to these five limestones,
362 MA stone is the only one showing the particularity of a residual expansion after a 1050 °C heating-
363 cooling cycle. This particularity, found during the repetition of three tests, seems to express an
364 advanced state of cracking of the material. GR siliceous stone shows very little residual deformation
365 up to 500 °C. However, an exposure to higher temperatures (750 and 1050 °C) results in a permanent
366 expansion. The evolution of the thermal deformation above 573 °C is directly related to the
367 reversibility of the α - β quartz phase transition. Thus, the path taken during the cooling phase is very
368 close to that shown during heating, contrary to the linear specificity shown by limestones.



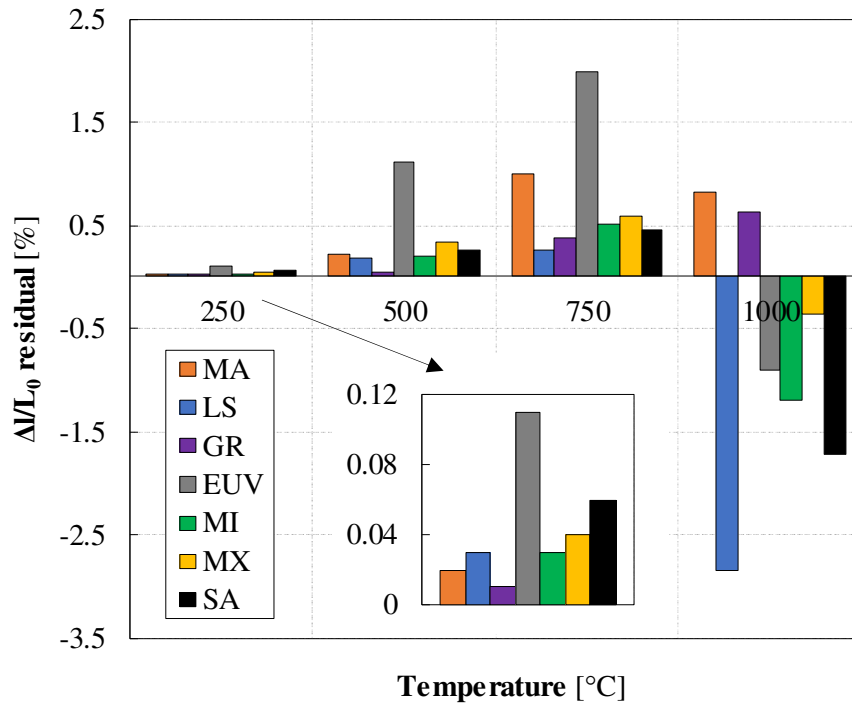
369

370 *Figure 9 - Individual curves of thermal deformation during the heating and cooling stages: influence*
 371 *of the maximum heating temperature T_{max} on the residual deformation*

372

373 A heating-cooling cycle at 250 °C induces very little residual deformation. However, EUV
374 limestone differs from other stones with a much higher value (0.12 %). After the 500 °C heating-
375 cooling cycle, the residual deformation of EUV become more pronounced, where a residual positive
376 deformation of 1.11 % is obtained. The sudden change in deformation kinetics observed at 400 °C
377 appears to produce advanced cracking in the material. In comparison, MX limestone, with the second
378 highest value, has only 0.33 %, while the other limestones range from 0.20 to 0.27 %. The GR
379 sandstone is slightly sensitive and its thermal deformation is almost reversible up to 500 °C. After a
380 heating-cooling cycle at 750 °C, several elements appear: EUV limestone continues to show a very
381 significant residual deformation (1.99 %), and MA stone stands out from other limestones, with a
382 significant increase in its value (1.00 %). The first peak detected (642 °C) on the evolution of its
383 thermal expansion coefficient may explain the sudden development of irreversible damage to the
384 material. The same observation can be made for the stones containing quartz, GR and MX, which
385 present a sudden expansion of this mineral at 573 °C, that can cause microcracking. Thus, GR
386 sandstone finally shows a certain residual deformation (0.38 %). The most porous limestones (MI, MX
387 and SA) display slightly higher values (~ 0.50 %). After this temperature level, LS limestone appears
388 to be the least sensitive stone with the lowest residual deformation (0.26 %). Among the other
389 monophasic limestones that contain only calcite (EUV, MI, SA), LS stone displays the best
390 mechanical performances at initial state. Thus, under equal loads, microcracking is lower in LS than in
391 other stones, resulting in a lower proportion of irreversible deformation. The highest temperature level
392 (1050 °C) leads to residual deformation that are no longer positive but negative for limestones, except
393 for MA stone. Indeed, the significant mass loss (44 %) resulting from the decomposition of calcite
394 leads to a more or less pronounced contraction, depending on the stone. LS stone, which was not very
395 sensitive so far, shows a relatively high contraction after cooling (2.85 %) in comparison to other
396 limestones (1.72 % for SA, 1.20 % for MI, 0.90 % for EUV and 0.36 % for MX). GR, which has the
397 specificity of a stable deformation after 573 °C, does not present a drastic change in its residual
398 deformation: 0.38 % after 750 °C and 0.62 % after 1000 °C.

399 It should be noted that an exposure to a temperature level that allows the beginning of calcite
400 decomposition (above 750 °C), and therefore the creation of lime, will bring about a certain instability
401 of the sample over time, after cooling. The formation of portlandite, through the rehydration of the
402 lime obtained ($\text{CaO} + \text{H}_2\text{O} \rightarrow \text{Ca(OH)}_2$) is associated with a high-volume expansion (44 %)
403 [3,9,16,50], increasing the cracking density of the sample.



404

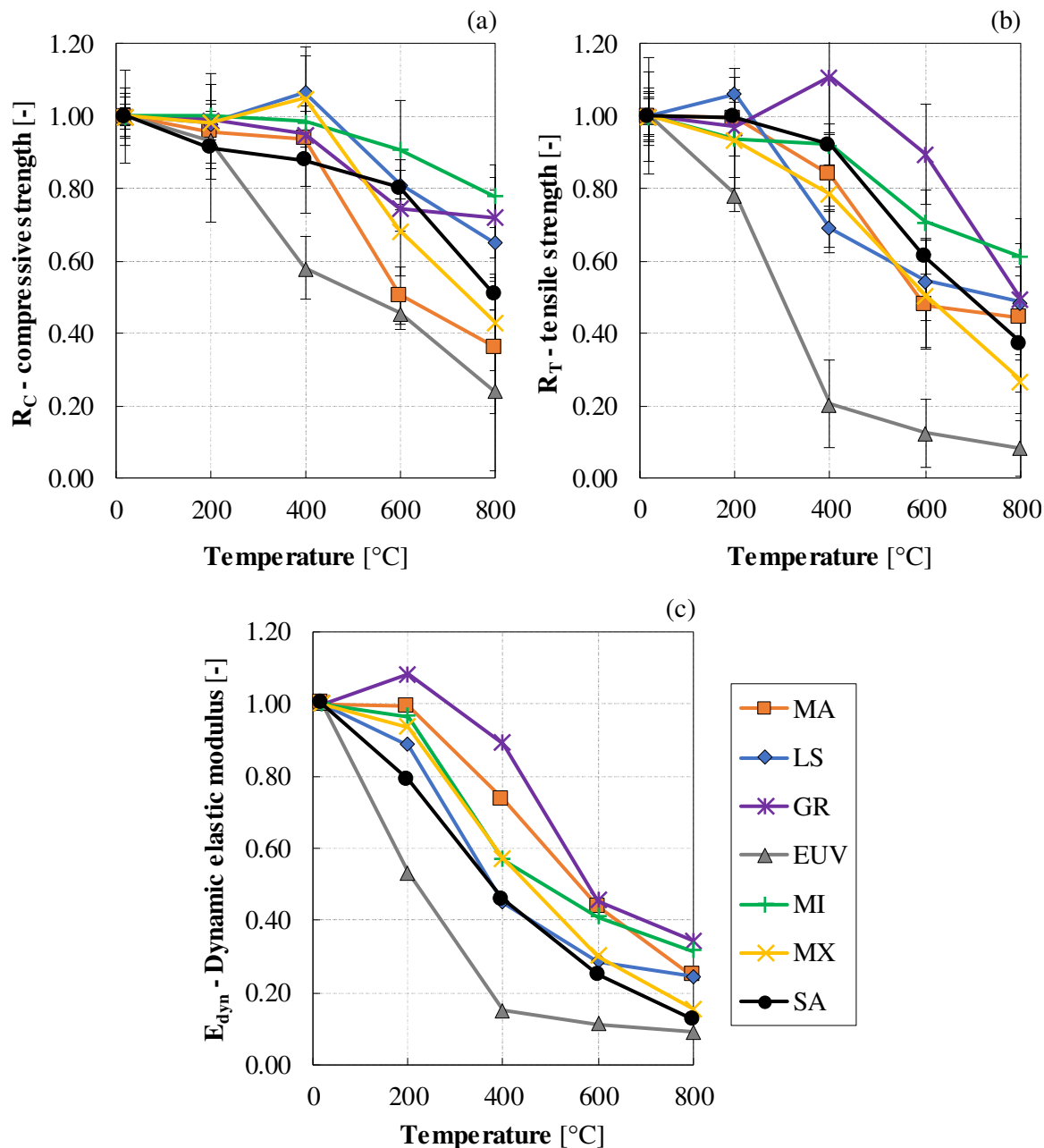
405 *Figure 10 - Comparison of the thermal residual deformations induced by different temperature levels*

406 **3.3 Effect of heating-cooling cycles on mechanical properties**

407 Figure 11 presents the relative evolution (final value/ initial value) of properties up to 800 °C:
 408 uniaxial compressive strength (R_C), indirect tensile strength (R_T), and dynamic elastic modulus (E_{dyn})
 409 after the four different heating-cooling cycles.

410 The mechanical parameters R_C and R_T seem to be only slightly affected by a heating-cooling
 411 cycle at 200 °C. Indeed, a maximum loss of 8 % is observable, except for EUV limestone, which
 412 therefore shows a significant drop of 22 % in tensile strength. This observation is even more
 413 pronounced for the dynamic elastic modulus (E_{dyn}): decrease up to 21 % for SA, and 47 % for EUV.
 414 After this first temperature level, the compressive strength and tensile strength show a different
 415 relative evolution. Thus, at 400 °C, the decrease in compressive strength does not exceed 12 % while
 416 the tensile strength decreases more significantly, between 8 % and 31 % for SA and LS respectively,
 417 and even more for EUV limestone with a significant reduction of 79 %. GR sandstone shows a slight
 418 increase (+ 11 %) in tensile strength, even though the dispersion of values does not allow this
 419 evolution to be assessed with certainty. At 600 and 800 °C, the overall trend appears similar for these
 420 two mechanical properties. GR sandstone and MI limestone are the least affected by these high
 421 temperature levels: loss of 20-30 % in compressive strength and 40-50 % in tensile strength at 800 °C.
 422 EUV limestone, which appears by far the most sensitive at high temperature, has a 76 % and 92 %

423 decrease in compressive and tensile strength respectively at 800 °C. The relative evolution of dynamic
 424 elastic modulus displays similar tendencies with a linear decrease along the temperature.



425
 426 *Figure 11 - Relative evolution of properties up to 800 °C: (a) uniaxial compressive strength R_C , (b)*
 427 *tensile strength R_T , and (c) dynamic elastic modulus E_{dyn}*

428 The analysis of the evolution of mechanical performances allows to establish a stones
 429 classification according to their level of sensitivity to high temperature. As mentioned above, MI and
 430 GR stones are defined as the most resistant. MI limestone with its very specific texture may explain its
 431 good mechanical behaviour at high temperature. Indeed, this isotropic and monophasic (calcite) stone,

432 composed mainly of a very fine micrite matrix, has very small grains. Thus, the absolute thermal
433 expansion shows lower amplitude, and associated with high porosity, the grains expand more freely
434 without generating strong mechanical stresses between the grains. Concerning GR sandstone, its good
435 mechanical behaviour above 600 °C may be explained by the fact that thermal deformation no longer
436 evolves at temperatures beyond 573 °C. Its thermal linear expansion coefficient is then almost zero up
437 to 1000 °C. Then, LS and SA limestones have a similar mechanical drop at 600 °C, but more
438 pronounced than MI and GR at 800 °C, specifically SA. This latter stone is associated with a grain size
439 (> 500 µm) far above LS (300 µm) and even higher than MI (< 100 µm). This characteristic, linked to
440 the strong presence of ooids in the stone, may explain this more pronounced sensitivity in comparison
441 with MI stone. This is also confirmed with the thermal residual deformation displayed by SA at 750
442 °C, which is slightly higher than LS. Then, MA and MX stones, with polyphasic mineralogical
443 composition, show sudden decrease in mechanical properties at 600 °C. The presence of quartz as
444 secondary mineral in these two stones may be a first explanation: the significant and almost
445 instantaneous volume expansion of the quartz grains, resulting from the polymorphic transition of this
446 mineral at 573 °C, seems to bring strong inequalities in deformation compared to calcite. This may
447 generate a high concentration of intergranular stresses, resulting in a densification of microcracks. In
448 addition, MA limestone is composed largely of dolomite, which start to decompose at 600 °C: these
449 grains are then in a contraction phase while calcite grains are in expansion phase. This leads again to
450 differential expansion problems increasing the cracking state of the sample. Previous results of
451 residual deformation showing a high value for MA stone at 750 °C confirm this statement. Finally,
452 EUV limestone is the least resistant stone even when it is exposed to a low temperature level (200 °C).
453 This stone already differed from the others by displaying very significant residual deformation. EUV
454 stone displays a very specific texture, composed of pluri-millimetric grains that are often in direct
455 contact with each other. Hence, the highly anisotropic expansion of calcite generates stresses
456 concentration between adjacent grains, resulting in cracking and loss of cohesion between the grains.

457 **4. Conclusion**

458 The high temperature behaviour of seven French natural building stones have been studied.
459 Firstly, tests under high temperature were conducted to identify the main mechanisms of alteration
460 such as thermo-chemical transformations but also thermal deformation. Then, tests were performed on
461 heated specimens after different heating-cooling cycles in order to investigate the evolution of
462 mechanical properties. The principal results of this work indicate that these limestones and sandstone
463 can be highly affected by high temperature exposure but may exhibit different behaviours:

- 464 – the mineralogical composition appears to play a major role in the thermal stability of
465 stones: limestones showed a mass loss due to calcite decarbonation, initiated at 750 °C
466 and resulting in 44 % at 930 °C. Furthermore, the presence of quartz has been identified
467 by endothermic peaks at 573 °C, but has not led to any mass loss. Lastly, a small
468 amount of organic matter in one specific limestone (EUV) led to a slight early mass loss
469 at 370 °C;
- 470 – several intrinsic parameters such as petrophysical (grain size, texture, initial porosity)
471 and mechanical properties displayed a strong influence on the thermal behaviour of
472 stones. Then, polyphasic stones composed of both calcite-dolomite (MA) or calcite-
473 quartz (MX) are more vulnerable to differential thermal deformation caused by different
474 thermal behaviours: it can generate internal stresses, which generally occur along the
475 grain boundaries, and therefore results in microcracking and granular disintegration.
476 Indeed, residual deformations observed after a 500 °C heating-cooling cycle show this
477 state of irreversible damage. Moreover, the stones with a coarse-grained texture (EUV)
478 are more sensitive than stones presenting a homogeneous distribution of small grains
479 associated with a fine micrite matrix (MI). Indeed, EUV limestone expanded widely and
480 displayed a significant irreversible deformation. The sandstone of this study (GR)
481 differs from limestones due to their low residual deformation linked with the reversible
482 polymorphic α - β quartz transition. However, quartz expand more than calcite but do not
483 present a large anisotropy as calcite;
- 484 – the evolution of mechanical properties up to 800 °C has been established. Although it is
485 difficult to generalize a trend in evolution to limestones, a rise in temperature leads to a
486 decrease in mechanical performances. However, when heated below 400 °C, there is not
487 a significant change in mechanical properties, except for EUV stone due to its specific
488 texture (weakly cemented) and an early mass loss (370 °C). Nevertheless, exposure to
489 higher temperatures bring an important drop in mechanical strengths. In addition, the
490 sandstone GR, which does not undergo major irreversible thermo-chemical
491 transformations, showed a good residual mechanical stability after cooling.

492 **5. Acknowledgements**

493 This research was supported by the “Fondation des Sciences du Patrimoine (ANR-10-LABX-
494 0094-01)”. The authors express their gratitude to this organization, and to Rocamat for providing the
495 stone samples.

6. References

- 497 [1] M. Gómez-Heras, S. McCabe, B.J. Smith, R. Fort, Impacts of fire on stone-built heritage : an
498 overview, *J. Archit. Conserv.* 15 (2009) 47–58.
499 <https://doi.org/10.1080/13556207.2009.10785047>.
- 500 [2] S. McCabe, B.J. Smith, P.A. Warke, Exploitation of inherited weakness in fire-damaged
501 building sandstone : the “fatiguing” of “shocked” stone, *Eng. Geol.* 115 (2010) 217–225.
502 <https://doi.org/10.1016/j.enggeo.2009.06.003>.
- 503 [3] M. Gómez-Heras, M. Álvarez de Buergo, R. Fort, M. Hajpál, Á. Török, M.J. Varas, Evolution
504 of porosity in Hungarian building stones after simulated burning, in: *Proc. Int. Conf. Heritage,*
505 *Weather. Conserv. HWC 2006, 2006:* pp. 513–519.
- 506 [4] V. Brotóns, R. Tomás, S. Ivorra, J.C. Alarcón, Temperature influence on the physical and
507 mechanical properties of a porous rock : San Julian’s calcarenite, *Eng. Geol.* 167 (2013) 117–
508 127. <https://doi.org/10.1016/j.enggeo.2013.10.012>.
- 509 [5] S. Chaki, M. Takarli, W.P. Agbodjan, Influence of thermal damage on physical properties of a
510 granite rock : porosity, permeability and ultrasonic wave evolutions, *Constr. Build. Mater.* 22
511 (2008) 1456–1461. <https://doi.org/10.1016/j.conbuildmat.2007.04.002>.
- 512 [6] A. Biró, V. Hlavička, É. Lublóy, Effect of fire-related temperatures on natural stones, *Constr.*
513 *Build. Mater.* 212 (2019) 92–101. <https://doi.org/10.1016/j.conbuildmat.2019.03.333>.
- 514 [7] S. Liu, J. Xu, An experimental study on the physico-mechanical properties of two post-high-
515 temperature rocks, *Eng. Geol.* 185 (2015) 63–70. <https://doi.org/10.1016/j.enggeo.2014.11.013>.
- 516 [8] R. Houpert, F. Homand-Etienne, Comportement mécanique des roches en fonction de la
517 température, *Rev. Française Géotechnique.* 28 (1979) 41–47.
- 518 [9] M.J. Heap, S. Mollo, S. Vinciguerra, Y. Lavallée, K.U. Hess, D.B. Dingwell, P. Baud, G. Iezzi,
519 Thermal weakening of the carbonate basement under Mt. Etna volcano (Italy) : implications for
520 volcano instability, *J. Volcanol. Geotherm. Res.* 250 (2013) 42–60.
521 <https://doi.org/10.1016/j.jvolgeores.2012.10.004>.
- 522 [10] A. Ozguven, Y. Ozcelik, Effects of high temperature on physico-mechanical properties of
523 Turkish natural building stones, *Eng. Geol.* 183 (2014) 127–136.
524 <https://doi.org/10.1016/j.enggeo.2014.10.006>.
- 525 [11] J. Sippel, S. Siegesmund, T. Weiss, K.-H. Nitsch, M. Korzen, Decay of natural stones caused
526 by fire damage, *Geol. Soc. London, Spec. Publ.* 271 (2007) 139–151.

- 527 <https://doi.org/10.1144/gsl.sp.2007.271.01.15>.
- 528 [12] A. Zeisig, S. Siegesmund, T. Weiss, Thermal expansion and its control on the durability of
529 marbles, *Geol. Soc. Spec. Publ.* 205 (2002) 65–80.
530 <https://doi.org/10.1144/GSL.SP.2002.205.01.06>.
- 531 [13] Z. Xing, R. Hébert, A.L. Beaucour, B. Ledésert, A. Noumowé, Influence of chemical and
532 mineralogical composition of concrete aggregates on their behaviour at elevated temperature,
533 *Mater. Struct.* (2013) 1921–1940. <https://doi.org/10.1617/s11527-013-0161-y>.
- 534 [14] W.S. González-Gómez, P. Quintana, A. May-Pat, F. Avilés, J. May-Crespo, J.J. Alvarado-Gil,
535 Thermal effects on the physical properties of limestones from the Yucatan Peninsula, *Int. J.*
536 *Rock Mech. Min. Sci.* 75 (2015) 182–189. <https://doi.org/10.1016/j.ijrmms.2014.12.010>.
- 537 [15] M. Hajpál, Á. Török, Mineralogical and colour changes of quartz sandstones by heat, *Environ.*
538 *Geol.* 46 (2004) 311–322. <https://doi.org/10.1007/s00254-004-1034-z>.
- 539 [16] Á. Török, M. Hajpál, Effect of temperature changes on the mineralogy and physical properties
540 of sandstones - A laboratory study, *Restor. Build. Monum.* 11 (2005) 1–8.
541 <https://doi.org/10.1515/rbm-2005-5969>.
- 542 [17] R.N. Razafinjato, A.L. Beaucour, R. Hébert, A. Noumowé, B. Ledésert, R. Bodet, Thermal
543 stability of different siliceous and calcareous aggregates subjected to high temperature,
544 *MATEC Web Conf.* 6 (2013) 1–9. <https://doi.org/10.1051/mateconf/20130607001>.
- 545 [18] R.N. Razafinjato, A.L. Beaucour, R. Hébert, B. Ledésert, R. Bodet, A. Noumowé, High
546 temperature behaviour of a wide petrographic range of siliceous and calcareous aggregates for
547 concretes, *Constr. Build. Mater.* 123 (2016) 261–273.
548 <https://doi.org/10.1016/j.conbuildmat.2016.06.097>.
- 549 [19] F. Robert, H. Colina, The influence of aggregates on the mechanical characteristics of concrete
550 exposed to fire, *Mag. Concr. Res.* 61 (2008) 311–321.
551 <https://doi.org/10.1680/macrc.2007.00121>.
- 552 [20] D. Richter, G. Simmons, Thermal expansion behavior of igneous rocks, *Int. J. Rock Mech.*
553 *Min. Sci.* 11 (1974) 403–411. [https://doi.org/10.1016/0148-9062\(74\)91111-5](https://doi.org/10.1016/0148-9062(74)91111-5).
- 554 [21] H.W. Cooper, G. Simmons, The effect of cracks on the thermal expansion of rocks, *Earth*
555 *Planet. Sci. Lett.* 36 (1977) 404–412. [https://doi.org/10.1016/0012-821X\(77\)90065-6](https://doi.org/10.1016/0012-821X(77)90065-6).
- 556 [22] J.J. de Castro Lima, A.B. Paraguassú, Linear thermal expansion of granitic rocks : influence of
557 apparent porosity, grain size and quartz content, *Bull. Eng. Geol. Environ.* 63 (2004) 215–220.

- 558 <https://doi.org/10.1007/s10064-004-0233-x>.
- 559 [23] V. Gräf, M. Jamek, A. Rohatsch, E. Tschegg, Effects of thermal-heating cycle treatment on
560 thermal expansion behavior of different building stones, *Int. J. Rock Mech. Min. Sci.* 64 (2013)
561 228–235. <https://doi.org/10.1016/j.ijrmms.2013.08.007>.
- 562 [24] Ö. Kiliç, The influence of high temperatures on limestone P-wave velocity and Schmidt
563 hammer strength, *Int. J. Rock Mech. Min. Sci.* 43 (2006) 980–986.
564 <https://doi.org/10.1016/j.ijrmms.2005.12.013>.
- 565 [25] A.S. Goudie, R.J. Allison, S.J. McLaren, The relations between modulus of elasticity and
566 temperature in the context of the experimental simulation of rock weathering by fire, *Earth
567 Surf. Process. Landforms.* 17 (1992) 605–615. [https://doi.org/10.1016/0148-9062\(93\)90761-2](https://doi.org/10.1016/0148-9062(93)90761-2).
- 568 [26] J. Rodríguez-Gordillo, M.P. Sáez-Pérez, Effects of thermal changes on Macael marble :
569 experimental study, *Constr. Build. Mater.* 20 (2006) 355–365.
570 <https://doi.org/10.1016/j.conbuildmat.2005.01.061>.
- 571 [27] G. Barbera, G. Barone, P. Mazzoleni, A. Scandurra, Laboratory measurement of ultrasound
572 velocity during accelerated aging tests : implication for the determination of limestone
573 durability, *Constr. Build. Mater.* 36 (2012) 977–983.
574 <https://doi.org/10.1016/j.conbuildmat.2012.06.029>.
- 575 [28] V. Pires, L.G. Rosa, A. Dionísio, Implications of exposure to high temperatures for stone
576 cladding requirements of three Portuguese granites regarding the use of dowel-hole anchoring
577 systems, *Constr. Build. Mater.* 64 (2014) 440–450.
578 <https://doi.org/10.1016/j.conbuildmat.2014.03.035>.
- 579 [29] E. Martinho, M. Mendes, A. Dionísio, 3D imaging of P-waves velocity as a tool for evaluation
580 of heat induced limestone decay, *Constr. Build. Mater.* 135 (2017) 119–128.
581 <https://doi.org/10.1016/j.conbuildmat.2016.12.192>.
- 582 [30] C. Walbert, J. Eslami, A.L. Beaucour, A. Bourgès, A. Noumowé, Evolution of the mechanical
583 behaviour of limestone subjected to freeze-thaw cycles, *Environ. Earth Sci.* 74 (2015) 6339–
584 6351. <https://doi.org/10.1007/s12665-015-4658-2>.
- 585 [31] T. De Kock, J. Dewanckele, M. Boone, G. De Schutter, P. Jacobs, V. Cnudde, Replacement
586 stones for Lede stone in Belgian historical monuments, *Geol. Soc. London.* 391 (2014) 31–46.
587 <https://doi.org/10.1144/SP391.9>.
- 588 [32] J. Eslami, C. Walbert, A.L. Beaucour, A. Bourgès, A. Noumowé, Influence of physical and
589 mechanical properties on the durability of limestone subjected to freeze-thaw cycles, *Constr.*

- 590 Build. Mater. 162 (2018) 420–429. <https://doi.org/10.1016/j.conbuildmat.2017.12.031>.
- 591 [33] M. Vigroux, J. Eslami, A.L. Beaucour, A. Bourgès, A. Noumowé, Experimental investigation
592 on physico-mechanical properties of natural building stones exposed to high temperature, in:
593 Proc. SMAR 2019, 5th Int. Conf. Smart Monit. Assess. Rehabil. Civ. Struct., 2019.
- 594 [34] P. Lopez-Arce, M. Tagnit-Hammou, B. Menendez, J.D. Mertz, M. Guiavarc'h, A. Kaci, S.
595 Aggoun, A. Cousture, Physico-chemical stone-mortar compatibility of commercial stone-repair
596 mortars of historic buildings from Paris, Constr. Build. Mater. 124 (2016) 424–441.
597 <https://doi.org/10.1016/j.conbuildmat.2016.07.076>.
- 598 [35] R.J. Dunham, Classification of carbonate rocks according to depositional texture, in: Classif.
599 Carbonate Rocks Am. Assoc. Pet. Geol. Mem., 1962: pp. 108–121.
600 <https://doi.org/10.1306/M1357>.
- 601 [36] R.H. Dott, Wacke, graywacke and matrix: what approach to immature sandstone
602 classification?, J. Sediment. Res. 34 (1964) 625–632. <https://doi.org/10.1306/74D71109-2B21-11D7-8648000102C1865D>.
- 604 [37] AFNOR, NF EN 1926, Méthodes d'essai des pierres naturelles - Détermination de la résistance
605 en compression uniaxiale, 2007.
- 606 [38] AFNOR, NF P 94-422, Roches - Détermination de la résistance à la traction - Méthode
607 indirecte - Essai brésilien, 2001.
- 608 [39] AFNOR, NF EN 1936, Méthodes d'essai des pierres naturelles - Détermination des masses
609 volumiques réelle et apparente et des porosités ouverte et totale, 2007.
- 610 [40] AFNOR, NF EN 14579, Méthodes d'essai pour pierres naturelles - Détermination de la vitesse
611 et propagation du son, 2005.
- 612 [41] RILEM, Rilem TC 129-MHT: Test methods for mechanical properties of concrete at high
613 temperatures - Compressive strength for service and accident conditions, Mater. Struct. 28
614 (1995) 410–414.
- 615 [42] A. Al-Omari, Evaluation des risques d'altération d'origine thermo-hydro-mécanique des
616 pierres du patrimoine bâti, PhD Thesis, Université d'Orléans, France, 2014.
- 617 [43] F. Homand-Etienne, Comportement mécanique des roches en fonction de la température, PhD
618 Thesis, Université de Nancy, France, 1986.
- 619 [44] N. Concha-Lozano, Compatibilité et durabilité des pierres de substitution dans les monuments -
620 Aspects physicochimiques et visuels, PhD Thesis, Ecole Nationale Supérieure des Mines de

- 621 Saint-Etienne, France, 2012.
- 622 [45] W.S. González-Gómez, P. Quintana, A. May-Pat, F. Avilés, J. May-Crespo, J.J. Alvarado-Gil,
623 Thermal effects on the physical properties of limestones from the Yucatan Peninsula, *Int. J.*
624 *Rock Mech. Min. Sci.* 75 (2015) 182–189. <https://doi.org/10.1016/j.ijrmms.2014.12.010>.
- 625 [46] M. Samtani, D. Dollimore, K.. Alexander, Comparison of dolomite decomposition kinetics
626 with related carbonates and the effect of procedural variables on its kinetic parameters,
627 *Thermochim. Acta.* 392–393 (2002) 135–145. [https://doi.org/10.1016/s0040-6031\(02\)00094-1](https://doi.org/10.1016/s0040-6031(02)00094-1).
- 628 [47] P. Hartlieb, M. Toifl, F. Kuchar, R. Meisels, T. Antretter, Thermo-physical properties of
629 selected hard rocks and their relation to microwave-assisted comminution, *Miner. Eng.* 91
630 (2016) 34–41. <https://doi.org/10.1016/j.mineng.2015.11.008>.
- 631 [48] R. Tiskatine, A. Eddemani, L. Gourdo, B. Abnay, A. Ihlal, A. Aharoune, L. Bourden,
632 Experimental evaluation of thermo-mechanical performances of candidate rocks for use in high
633 temperature thermal storage, *Appl. Energy.* 171 (2016) 243–255.
634 <https://doi.org/10.1016/j.apenergy.2016.03.061>.
- 635 [49] A. V. Denisov, A. Sprince, Analytical determination of thermal expansion of rocks and
636 concrete aggregates, *Mag. Civ. Eng.* 80 (2018) 151–170. <https://doi.org/10.18720/MCE.80.14>.
- 637 [50] B. Chakrabarti, T. Yates, A. Lewry, Effect of fire damage on natural stonework in buildings,
638 *Constr. Build. Mater.* 10 (1996) 539–544. [https://doi.org/10.1016/0950-0618\(95\)00076-3](https://doi.org/10.1016/0950-0618(95)00076-3).
- 639